Int. J. Fuzzy Syst. (2020) 22(1):181–200
https://doi.org/10.1007/s40815-019-00780-1

General Type-2 Fuzzy Gain Scheduling PID Controller with Application to Power-Line Inspection Robots

Tao Zhao[1] · Yao Chen[1] · Songyi Dian[1] · Rui Guo[2] · Shengchuan Li[3]

Received: 3 June 2019 / Revised: 15 October 2019 / Accepted: 26 November 2019 / Published online: 9 December 2019

Abstract In this paper, a general type-2 fuzzy gain scheduling PID (GT2FGS-PID) controller is presented to achieve self-balance adjustment of the power-line inspection (PLI) robot system. As the PLI robot system is an under-actuated nonlinear system, obtaining the full information of the four-state variables is necessary to balance the PLI robot. However, as the number of input variables increases, the number of control rules increases exponentially, making the design of the fuzzy controller extremely complex. Therefore, the proposed controller prevents the problem of rule explosion using information fusion and then simplifies the control design. Moreover, the particle swarm optimization algorithm is used to select improved controller parameters and make the controller achievable. In this paper, the control performance and anti-interference ability of the traditional PID control, type-1 fuzzy control, interval type-2 fuzzy control, and general type-2 fuzzy control methods are compared. By means of numerical simulation, we can conclude that the GT2FGS-PID controller exhibits superior stability and robustness over other controllers for the PLI robot system.

Keywords General type-2 fuzzy gain scheduling PID controller · Balance control · Inspection robot · Nonlinear under-actuated system

1 Introduction

As its name suggests, a power-line inspection (PLI) robot performs the inspection of outdoor, high-voltage equipment at substations, either autonomously or remotely. It is responsible for checking the internal thermal defects of the power equipment, external mechanical or electrical problems, such as foreign matter, damage, heat, and other issues, and then providing operators with relevant data to diagnose potential accidents in the operation of power equipment. One of the reasons that intelligent robot research is so popular is that intelligent robots offer numerous advantages, such as less manpower consumption and longer working hours. Another important reason is that they can replace human beings to perform a great deal of dangerous work, such as power inspection, as mentioned in this paper [1–5]. To reduce the cost and weight, and enhance the system flexibility, the PLI robot adopts an under-actuated structure, so there is no doubt that its controller design is more complicated than the full driving system [6, 7].

Several main approaches are available to control the under-actuated nonlinear system, such as backstepping control (BC) [7, 8], sliding mode control (SMC) [9], the

✉ Songyi Dian
songyi_dian@126.com

Tao Zhao
zhaotaozhaogang@126.com

Yao Chen
2017223035189@stu.scu.edu.cn

Rui Guo
guoruihit@gmail.com

Shengchuan Li
lnlsc@163.com

[1] College of Electrical Engineering, Sichuan University, Chengdu 610065, China

[2] State Grid Shandong Electric Power Company, Jinan 250001, China

[3] Electric Power Research Institute of State Grid Liaoning Electric Power Co., Ltd., Shenyang 110006, China

energy method [10], and adaptive control [11–14]. These methods each exhibit their own applicability and limitations. For example, BC has achieved effective results in controlling the PLI robot, but the control method was developed based on the linear model of the PLI robot. In other words, it is difficult to control under-actuated nonlinear systems [7, 8]. SMC is superior in terms of the dynamic adjustment process, but it is complex to identify a suitable SMC law, and it has limited capacity for handling high-order uncertainty. As the PLI robot is an under-actuated nonlinear system and is faced with many uncertainties when working on high-voltage lines, improving the controller ability to deal with the uncertain under-actuated nonlinear PLI robot system remains a challenging task.

The traditional PID controller is still used extensively in modern industry, owing to its advantages of mature theory, simple operation, and appropriate price [15]. However, conventional PID controllers are unsatisfactory when the system to be controlled has a high level of complexity, such as nonlinearities, time delay, imprecise mathematical models, and structural uncertainties [16]. Moreover, PID controllers cannot easily deal with under-actuated nonlinear systems. Therefore, numerous researchers have attempted to combine a traditional PID controller with a fuzzy logic controller (FLC) to improve the controller ability to handle various types of uncertain under-actuated nonlinear systems. Several common structures exist for fuzzy PID controllers, including the fuzzy PI, fuzzy PD, and fuzzy PID controllers [17–20]. These controllers with different structures have been applied to various subjects and have obtained superior control performance over conventional PID controllers. However, whether the traditional fuzzy PID controller is still effective in the presence of many uncertainties remains to be solved.

Many uncertainties exist when a PLI robot is working on a high-voltage line, including continuous external disturbances caused by the weather, and model uncertainties caused by machine wear. However, the ability of the type-1 fuzzy logic system (T1-FLS) to deal with a high level of uncertainties is limited, because its membership degrees are totally crisp [21]. As an extension of the T1-FLS, the interval type-2 fuzzy logic system (IT2-FLS) introduces uncertainty into the fuzzy set, which improves the anti-noise and unknown data processing abilities of the system. With respect to applications in which the IT2-FLS outperforms the T1-FLS, a multitude of related research is available [22–37]. As an extension of the IT2-FLS, the general type-2 fuzzy logic system (GT2-FLS) exhibits improvements over the IT2-FLS. In comparison with IT2-FLS, in which the uncertainty is represented as an area, the uncertainty is described by a volume in the GT2-FLS. Therefore, the GT2-FLS can better handle uncertainty [38, 39]. Similarly, a multitude of related researches and applications on the GT2-FLS are available [40]; for example, a new approach for reducing the computational cost of the GT2-FLS [41], a general type-2 fuzzy logic approach for dynamic parameter adaptation [42], controlling a mobile robot using the general type-2 fuzzy logic controller (GT2-FLC) [38], application of the adaptive GT2-FLC for nonlinear uncertain systems [43], a GT2-FLC with applications to aerospace [44], and type-2 fuzzy logic aggregation of multiple fuzzy controllers for airplane flight control [45]. With the advancement of the GT2-FLC, high-order uncertainty and uncertain noise can be handled better.

It can be observed from the above that the GT2-FLC has stronger anti-interference ability and can deal with various uncertainties compared with the T1-FLC and IT2-FLC. Therefore, it has advantages in practical application. The PLI robot system has been working under various high-order uncertainties for a long time, which requires the controller to be able to deal with high-order uncertainties. In addition, we need to pay attention to the fact that the parameters of the controller are calculated by PSO algorithm for offline optimization. Therefore, whether the optimized parameters can adapt to the application situation is still a challenge. However, the GT2-FLC can prevent this problem from two aspects as far as possible: first, the GT2-FLC does not rely on accurate mathematical models, so the controller can deal with the problem of parameter perturbation in the machine. Second, GT2-FLC can still maintain good control performance in the face of high-order uncertainty, which ensures that the controller can maintain the control performance consistent with the numerical simulation stage as far as possible in practical applications. Therefore, the GT2-FLC is considered in this paper.

First, the traditional PID controller has a limited ability to deal with uncertainty, while the GT2-FLC has superior capability of handling different types of uncertainties [46, 47]. The fuzzy rules of the GT2-FLC mostly originate from expert experience, which is difficult to obtain in the face of complex systems, while the PID control theory is mature, and rules can be designed through the regulation of parameters. Therefore, this study proposes the GT2FGS-PID controller and applies it to the PLI robot system.

The major contributions of this study are as follows: (1) The GT2FGS-PID controller is applied to the PLI robot to handle various types of uncertainties for the first time, including model uncertainties, external disturbances, and parameter perturbations supported by mechanical wear. As mentioned previously, the BC and SMC are generally used to control PLI robots with a linear model form, while the GT2-FLC is used to control PLI robots with a general nonlinear form. For example, in paper [8], adaptive gain-scheduled backstepping control is used, which is aimed at the linear model form and has weak anti-interference

ability. (2) Information fusion technology is adopted to prevent the problem of rule explosion in the GT2-FLS, which combines the information of four-state variables into two input variables, thus the rules of the controller are more convenient to adjust, and the controller is easier to realize. (3) The control performance and anti-interference ability of the traditional PID, type-1 fuzzy control, interval type-2 fuzzy control, and general type-2 fuzzy control methods are compared, and the simulation results demonstrate that the GT2FGS-PID controller is superior in the uncertain PLI robot system.

The remainder of this paper is organized as follows. The preliminaries are introduced in Sect. 2. In Sect. 3, the description of the PLI robot system is presented. The design and analysis of the GT2FGS-PID controller for the PLI robot system are demonstrated in Sect. 4. In Sect. 5, the simulation results of several cases of the PLI robot system are provided. The conclusion and future work are presented in Sect. 6.

2 Preliminaries

In this section, T1-FLS, IT2-FLS, and GT2-FLS are described.

2.1 Type-1 Fuzzy Inference Systems

Figure 1 presents a block diagram of the T1-FLS, which describes the main sections of the T1-FLS. It can be observed that five components exist: a fuzzifier, an inference engine, a rule base, and a defuzzifier [22].

A type-1 fuzzy set (T1-FS) A can be denoted by Eq. (1), where X is the universe for x, $x \in X$, and $\mu_A(x)$ is the degree of membership corresponding to x, which takes on a value in the interval [0,1]. It is worth noting that the membership function of T1-FS is often a convex function. Triangular, trapezoidal, and Gaussian membership functions are commonly used. Figure 2 illustrates the membership function of a triangle.

$$A = \{(x, \mu_A(x)) | x \in X\}. \tag{1}$$

The structure of the fuzzy rule for a T1-FLS is defined as Eq. (2), where R^l is a specific rule, x_p is the input p, F_p^l is a type-1 membership function of the input p on rule l, and y is the output on the membership function G^l.

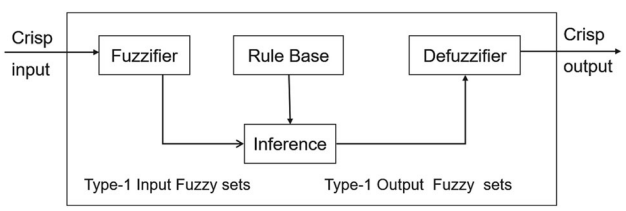

Fig. 1 Block diagram describing T1-FLS

$$\begin{aligned} &R^l: \text{IF } x_1 \text{ is } F_1^l \text{ and } \ldots \text{ and } x_p \text{ is } F_p^l, \\ &\text{THEN } y \text{ is } G^l, \text{ where } l = 1, \ldots M. \end{aligned} \tag{2}$$

The inference engine takes the form of Eq. (3) when the t-norm connectors (★) are used. Here, μ_{B^l} is the resulting membership function in the consequents per each rule inference, and Y is the output space belonging to the consequents.

$$\begin{aligned} \mu_{B^l}(y) = \mu_{G^l}(y) \bigstar \{ [\sup_{x_1 \in X_1} \mu_{x_1}(x_1) \bigstar \mu_{F_1^l}(x_1)] \\ \bigstar \ldots \bigstar [\sup_{x_p \in X_p} \mu_{x_p}(x_p) \bigstar \mu_{F_p^l}(x_p)] \}, \ y \in Y. \end{aligned} \tag{3}$$

Finally, the defuzzification process can be achieved in multiple manners: the centroid, center-of-sums, or heights defuzzifier methods are commonly used, and described by Eqs. (4) to (6), respectively. Here, y_i is the discrete position and $y_i \in Y$, $\mu_B(y_i)$ is the corresponding membership degree, c_{B^l} is the centroid on the lth output, a_{B^l} is the area of the set, and $\bar{y}^l$ is the point with the largest membership value in the lth output set, while $\mu_{B^l}(\bar{y}^l)$ is the corresponding membership degree.

$$y_c(x) = \frac{\sum_{i=1}^{N} y_i \mu_B(y_i)}{\sum_{i=1}^{N} \mu_B(y_i)} \tag{4}$$

$$y_a(x) = \frac{\sum_{l=1}^{M} c_{B^l} a_{B^l}}{\sum_{l=1}^{M} a_{B^l}} \tag{5}$$

$$y_h(x) = \frac{\sum_{l=1}^{M} \bar{y}^l \mu_{B^l}(\bar{y}^l)}{\sum_{l=1}^{M} \mu_{B^l}(\bar{y}^l)}. \tag{6}$$

The centroid defuzzifier is generally difficult and time consuming to compute, and therefore, it is not as widely used as it once was. However, the center-of-sums is much easier to compute than the centroid defuzzifier. Although the height defuzzifer is much easier to compute than the centroid defuzzfier, a problem may occur when a consequent set has its maximum value as $y = 0$ (this may occur for a left shoulder membership function that is a negatively sloping line with its maximum value at $y = 0$), in which case $\bar{y}^l = 0$. This means that such a rule has never contributed anything to $y_h(x)$, which appears unreasonable [48].

2.2 Interval Type-2 Fuzzy Inference Systems

As an extension of the T1-FLS, the IT2-FLS can handle higher uncertainty directly. Figure 3 illustrates the structure of the IT2-FLS. It is clear that the main difference

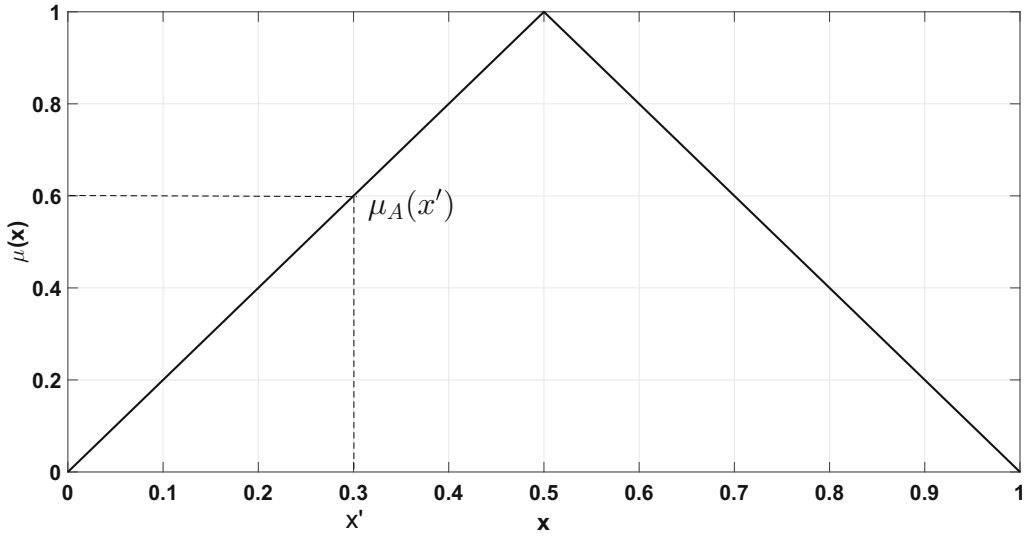

Fig. 2 T1-FS

from the T1-FLS is the defuzzification process, in which an IT2-FLS must first be simplified into a T1-FLS by a type-reducer, following which a crisp output can be obtained by the defuzzifier.

An interval type-2 fuzzy set (IT2-FS) $\tilde{A}$, which is a special case of the general type-2 fuzzy set (GT2-FS), can be denoted by Eq. (7), where x is the primary variable and has the domain X; u is the secondary variable, and has the domain J_x at each $x \in X$; J_x is known as the primary membership of x and is defined by Eq. (11); and the secondary membership grades of $\tilde{A}$ are all equal to 1 [49]. In this case, Fig. 4 illustrates a sample of IT2-FS. As indicated in Fig. 4, the uncertainty about $\tilde{A}$ is conveyed by the union of all primary memberships and represented by the blue area, suggesting that it has the ability to deal with uncertainty directly. This area is known as the footprint of uncertainty (FOU) of $\tilde{A}$, which is defined by Eq. (8).

$$\tilde{A} = \int_{x\in X} \int_{u\in J_x\subseteq[0,1]} 1/(x,u) = \int_{x\in X} \left[\int_{u\in J_x\subseteq[0,1]} 1/u \right] \Big/ x. \tag{7}$$

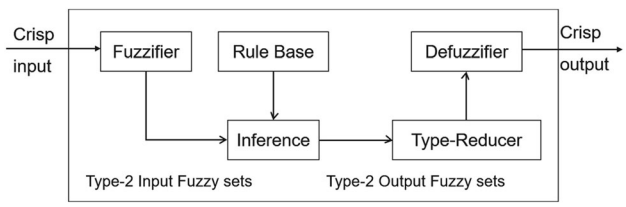

Fig. 3 Block Diagram Describing IT2-FLS

$$\mathrm{FOU}(\tilde{A}) = \bigcup_{\forall x\in X} J_x = \{(x,u) : u \in J_x \subseteq [0,1]\}. \tag{8}$$

The upper membership function (UMF) is associated with the upper bound of FOU($\tilde{A}$), and is denoted by $\bar{\mu}_{\tilde{A}}(x)$, $\forall x \in X$, while the lower membership function (LMF) is associated with the lower bound of FOU($\tilde{A}$), and is denoted by $\underline{\mu}_{\tilde{A}}(x)$, $\forall x \in X$; that is [50],

$$\overline{\mu}_{\tilde{A}(x)} = \overline{\mathrm{FOU}(\tilde{A})} \quad \forall x \in X. \tag{9}$$

$$\underline{\mu}_{\tilde{A}}(x) = \underline{\mathrm{FOU}(\tilde{A})} \quad \forall x \in X. \tag{10}$$

Note that J_x is an interval set, namely

$$J_x = \{(x,u) : u \in [\underline{\mu}_{\tilde{A}}, \bar{\mu}_{\tilde{A}}]\}. \tag{11}$$

The structure of the fuzzy rule for the IT2-FLS is similar to that of the TI-FLS, and is expressed as Eq. (12).

$$\begin{aligned} &R^l : \text{IF } x_1 \textit{ is } \tilde{F}_1^l \text{ and } \ldots \text{ and } x_p \text{ is } \tilde{F}_p^l, \\ &\text{THEN } y \text{ is } \tilde{G}^l, \text{ where } l = 1, \ldots M. \end{aligned} \tag{12}$$

The inference of the IT2-FLS can be represented by Eq. (14), where $\underline{f}^l$ and $\overline{f}^l$ are the firing sets, and are defined as Eqs. (14) and (15), respectively.

$$\mu_{\tilde{B}}(y) = \int_{b\in[(\underline{f}^1 \star \underline{\mu}_{\tilde{G}^1}(y)) \vee \ldots \vee (\underline{f}^N \star \underline{\mu}_{\tilde{G}^N}(y)), (\overline{f}^1 \star \overline{\mu}_{\tilde{G}^1}(y)) \vee \ldots \vee (\overline{f}^N \star \overline{\mu}_{\tilde{G}^N}(y))]} 1/b, y \in Y \tag{13}$$

and

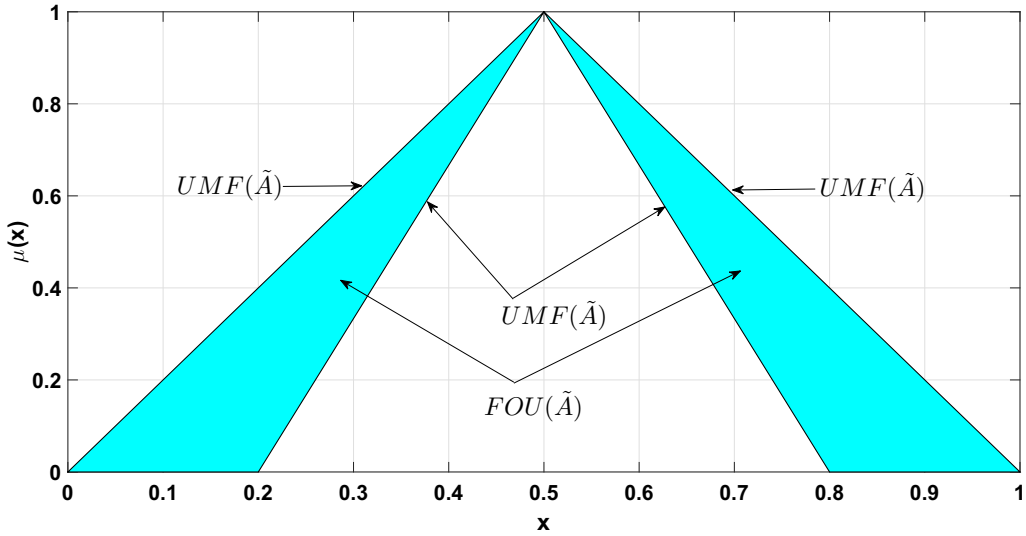

Fig. 4 IT2-FS

$$\underline{f}^{l}(\mathbf{x}') = \underline{\mu}_{\mathbf{F}_1^{\dagger}}(\mathbf{x_1}')\bigstar\ldots\bigstar\underline{\mu}_{\mathbf{F}_p^{\dagger}}(\mathbf{x_p}'). \tag{14}$$

$$\overline{f}^{l}(\mathbf{x}') = \overline{\mu}_{\mathbf{F}_1^{\dagger}}(\mathbf{x_1}')\bigstar\ldots\bigstar\overline{\mu}_{\mathbf{F}_p^{\dagger}}(\mathbf{x_p}'). \tag{15}$$

Type reduction, which is an extension of type-1 defuzzification, represents a mapping from T2-FS to T1-FS [31], and can be achieved by multiple means, one of these methods being that of the center-of-sets (COS), as indicated in Eq. (16). This reduction can save on computation time. It should be noted that $Y_{\cos}(x')$ is also an interval fuzzy set [51].

$$\begin{cases} Y_{\cos}(x') & = 1/[y_l(x'), y_r(x')] \\ y_l(x') & = \min\limits_{\forall w_s \in [\underline{f}^s(x'), \overline{f}^s(x')]} \sum\limits_{s=1}^{M} l_{\tilde{G}^s} w_s / \sum\limits_{s=1}^{M} w_s \\ y_r(x') & = \max\limits_{\forall w_s \in [\underline{f}^s(x'), \overline{f}^s(x')]} \sum\limits_{s=1}^{M} r_{\tilde{G}^s} w_s / \sum\limits_{s=1}^{M} w_s. \end{cases} \tag{16}$$

Finally, a crisp output value can be obtained by the defuzzification process, as denoted by Eq. (17).

$$y(x) = \frac{y_l + y_r}{2}. \tag{17}$$

2.3 General Type-2 Fuzzy Inference Systems

The logic structure of the GT2-FLS is the same as that of the IT2-FLS, with a minor difference in the calculation. The structure of the GT2-FLS can be represented by Fig. 3.

A GT2-FS $\tilde{\tilde{A}}$ can be described by Eq. (18), where $J_x^u \in [0, 1]$, x is the primary variable and u is the secondary variable. In this case, Fig. 5 illustrates the various elements of a GT2-FS, the secondary membership function of which is the triangle function.

$$\tilde{\tilde{A}} = \int_x \mu_{\tilde{\tilde{A}}}(x)/x = \int_x \left[\int_{J_x^u} f_x(u)/u\right]/x. \tag{18}$$

The rules for the GT2-FLS are the same as those for the IT2-FLS, with a difference in the notation, as indicated in Eq. (19).

$$\begin{aligned} &R^l : \text{IF } x_1 \text{ is } \tilde{\tilde{F}}_1^l \text{ and } \ldots \text{ and } x_p \text{ is } \tilde{\tilde{F}}_p^l, \\ &\text{THEN } y \text{ is } \tilde{\tilde{G}}^l, \text{ where } l = 1, \ldots M. \end{aligned} \tag{19}$$

The inference of a GT2-FLS can be simplified into two main operations, namely meet and join, as indicated in Eqs. (20) and (21) [38, 49].

$$\mu_{\tilde{\tilde{A}}} \sqcup \mu_{\tilde{\tilde{B}}} = \left\{\left[\int_{u\in J_x^u}\int_{u\in J_x^w} f_x(u)\bigstar g_x(w)/(u \vee w)\right]\right\} \tag{20}$$

$$\mu_{\tilde{\tilde{A}}} \sqcap \mu_{\tilde{\tilde{B}}} = \left\{\left[\int_{u\in J_x^u}\int_{u\in J_x^w} f_x(u)\bigstar g_x(w)/(u \wedge w)\right]\right\}. \tag{21}$$

The GT2-FS is substantially more complex than the IT2-FS and T1-FS. To make the GT2-FS calculation easier, several simplified representations have been proposed to avoid various computational problems [52, 53].

In this paper, the GT2-FS is denoted by the α-plane method [54]. The α-plane can be defined as follows:

$$\tilde{A}_\alpha = \int_{\forall x\in X}\int_{\forall u\in[0,1]} \{(x, u)|f_x(u) \geqslant \alpha\}. \tag{22}$$

When an α-plane is calculated, we can use the inference of an IT2-FS to reduce the complexity of the GT2-FS. The formulae for the α-cuts of the triangle secondary membership functions can be computed as follows [55]:

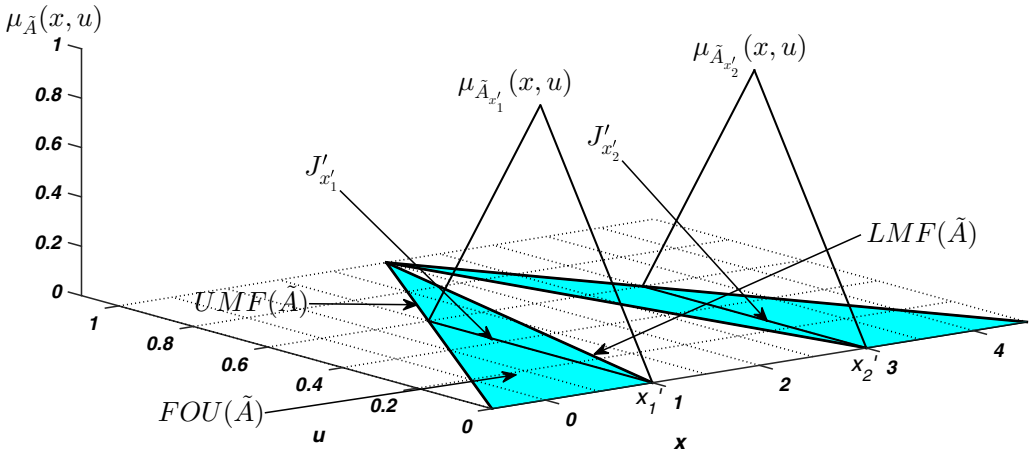

Fig. 5 Various Elements of GT2-FS

$$\begin{cases} \tilde{A_\alpha}(x) & = [a_\alpha(x), b_\alpha(x)] \\ a_\alpha(x) & = \underline{\mu}_{\tilde{A}}(x) + w[\overline{\mu}_{\tilde{A}}(x) - \underline{\mu}_{\tilde{A}}(x)]\alpha \\ b_\alpha(x) & = \overline{\mu}_{\tilde{A}}(x) - (1-w)[\overline{\mu}_{\tilde{A}}(x) - \underline{\mu}_{\tilde{A}}(x)]\alpha \end{cases}, \tag{23}$$

where w is the weight that determines the shape of the triangle secondary membership functions. Because the more α-planes are selected, the more accurate the representation of GT2-FLC membership function can be, the more accurate the control output can be calculated, and the better the controller performance can be realized. However, the increase in the number of α-planes also means the increase in the amount of computation, so we chose five representative α-planes to represent the GT2-FLC membership function to achieve a balance between computational complexity and controller performance.

3 PLI Robot System

The mathematical model of the PLI robot system in this section is mainly referenced from [7, 8]. The structure of the PLI robot is presented in Fig. 6. Moreover, Fig. 7 illustrates the balance adjustment parameters of the PLI robot. The Euler–Lagrange equation is considered to derive the dynamic model of the PLI robot system, and this equation can be defined by Eq. (24) [56].

$$U_i = \frac{\mathrm{d}}{\mathrm{d}t}\left[\frac{\partial L}{\partial \dot{\theta}_i}\right] - \frac{\partial L}{\partial \theta_i} \quad i = 1, \ldots, m \tag{24}$$

$$L = K - P, \tag{25}$$

where U_i is the torque acting on the ith generalized coordinate, θ_1 is the angle between the cable and PLI robot body, and θ_2 is the angle of rotation of the active joint. Furthermore, K is the kinetic energy of the PLI robot, while

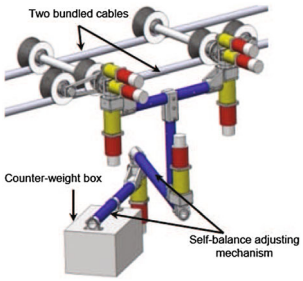

Fig. 6 Overall structure and operation mode of PLI robot

P is the potential energy of the PLI robot, and K and P can be denoted by Eqs. (26) and (27), respectively.

$$K = \frac{m_1 h_1^2 \dot{\theta}_1^2}{2} + \frac{m_2 l^2 \dot{\theta}_2^2}{2} + \frac{m_2[d^2 + (-h_{20} + l\sin\theta_2)]\dot{\theta}_1^2}{2} \tag{26}$$

$$P = -m_1 g h_1 \sin\theta_1 + m_2 g[-h\cos\theta_1(h_{20} + l\sin\theta_2)\sin\theta_1], \tag{27}$$

where g represents the acceleration of gravity. From Table 1, we can obtain

$$m_1 h_1 = m_2 h_{20}. \tag{28}$$

From Eqs. (27) and (28), P can be expressed as Eq. (29):

$$P = m_2 g(-d\cos\theta_1 + l\sin\theta_2\sin\theta_1). \tag{29}$$

The motion equation of the PLI robot can be obtained by Eq. (30). As the PLI robot system is an under-actuated system, τ_1 is equal to 0 in the absence of external disturbance. It can be observed from Figs. 6 and 7 that the PLI robot adjusts the center of gravity of the counter-weight by the self-balancing mechanism, and the balance is achieved

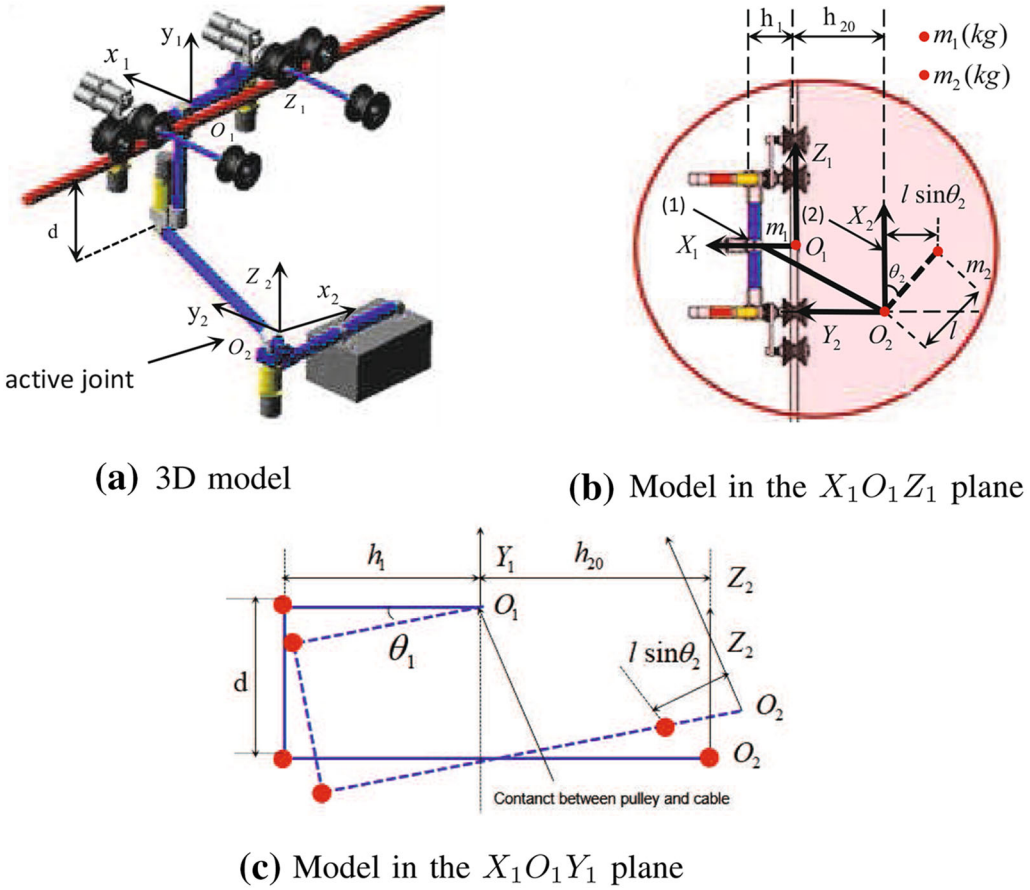

(a) 3D model

(b) Model in the $X_1O_1Z_1$ plane

(c) Model in the $X_1O_1Y_1$ plane

Fig. 7 Overall framework and corresponding parameters of PLI robot

Table 1 Structural parameters of PLI robot

Symbol	Parameter name	Value	Unit
m_1	Mass of PLI robot body	63	kg
m_2	Mass of counter-weight box	27	kg
h_1	Distance between cable and center of mass of body	0.18	m
h_{20}	Distance from cable to center of mass of counter-weight box	0.42	m
d	Height of T-shaped base	0.5	m
l	Length of the actuator bar	0.5	m
τ_1	External disturbance		N m
u_2	Torque applied to active joint θ_2		N m

by matching the center of gravity of the body and center of gravity of the counter-weight.

$$\begin{aligned}\tau_1 &= [m_1{h_1}^2 + m_2(d^2 + (-h_{20} + l\sin\theta_2)^2)\ddot{\theta_1}] \\ &\quad + 2m_2l(-h_{20} + l\sin\theta_2)(\cos\theta_2)\dot{\theta_1}\dot{\vartheta_2} \\ &\quad + m_2gd\sin\theta_1 + m_2gl\sin\theta_2\cos\theta_1 \\ u_2 &= m_2l^2\ddot{\theta_2} - m_2l(-h_{20} + l\sin\theta_2)(\cos\theta_2)\dot{\theta_1^2} \\ &\quad + m_2gl\cos\theta_2\sin\theta_1\end{aligned} \tag{30}$$

To provide an improved description of the motion process, the state variable vector is defined as follows:

$$x = [x_1\ x_2\ x_3\ x_4]^{\mathrm{T}} = [\theta_1\ \dot{\theta_2}\ \theta_2\ \dot{\theta_2}]^{\mathrm{T}}. \tag{31}$$

The parameters of the PLI robot are displayed in Table 1. The state space model of the PLI robot can be expressed as follows:

$$
\begin{aligned}
\dot{x_1} &= x_2 \\
\dot{x_2} &= \frac{\tau_1 - 2m_2 l(-h_{20} + l\sin x_3)(\cos x_3)x_2 x_4)}{[m_1 {h_1}^2 + m_2(d^2 + (-h_{20} + l\sin x_3)^2)]} \\
&\quad - \frac{m_2 g d \sin x_1 + m_2 g l \sin x_3 \cos x_1}{[m_1 {h_1}^2 + m_2(d^2 + (-h_{20} + l\sin x_3)^2)]} \\
\dot{x_3} &= x_4 \\
\dot{x_4} &= \frac{u_2 + m_2 l(-h_{20} + l\sin x_3)(\cos x_3 {x_2}^2))}{m_2 l^2} \\
&\quad - \frac{m_2 g l \cos x_3 \sin x_1}{m_2 l^2}.
\end{aligned} \tag{32}
$$

Remark 1 The nonlinear dynamic mathematical model is established for the PLI robot system. However, owing to the complexity of the PLI robot system, there remain many uncertainties that are ignored. The controller design based on the above model may not be applicable to the actual system. On this basis, in the following section, the GT2FGS-PID controller that does not depend entirely on the precise mathematical model is proposed, which has the potential to improve the ability of the controller to deal with uncertainties.

4 Design and Analysis of GT2FGS-PID Controller for PLI Robot System

4.1 Structure of the GT2FGS-PID Controller

The structure of the GT2FGS-PID controller is presented in Fig. 8. As illustrated in Fig. 8, the upper-lever controller of the system is the GT2-FLC, while the lower-lever controller is the traditional PID controller. The upper-lever controller selects parameters online by means of decision-making, and transmits the parameters to the PID controller, while the lower-level controller acts directly on the plant model.

The PID controller can be represented by Eq. (33).

$$
\begin{aligned}
u(t) &= k_p e(t) + k_i \int_0^t e(t')\mathrm{d}t' + k_d \frac{de(t)}{\mathrm{d}t} \\
e(t) &= y_r(t) - y_m(t),
\end{aligned} \tag{33}
$$

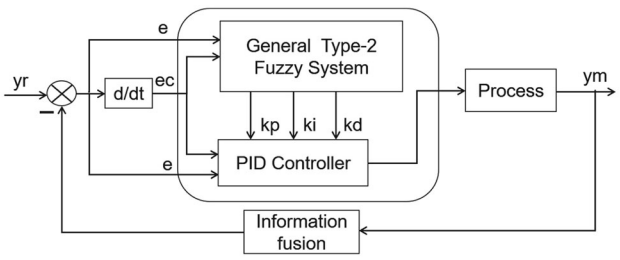

Fig. 8 Block diagram of GT2FGS-PID controller structure

where the proportion gain, integral gain, and derivative gain of the controller are denoted by k_p, k_i, and k_d, respectively. Furthermore, $u(t)$, $y_r(t)$, and $y_m(t)$ are the controller output, reference input, and system output, respectively. Usually, the values of k_p, k_i, and k_d are adjusted according to the system error $e(t)$ and error change rate $ec(t)$ ($de(t)/\mathrm{d}t$). These PID parameters can be adjusted online by developing the rule-based GT2-FLC structure [22].

As the PID controller is well known, later parts mainly introduce the knowledge of the fuzzy logic system. There are two types of fuzzy logic systems, namely the T-S fuzzy logic system [57] and Mamdani fuzzy logic system, and the Mamdani fuzzy logic system is adopted in this study.

4.2 Design and Implementation of the GT2FGS-PID Controller

First, for the two- level system, if the traditional Mamdani fuzzy controller is used to design the four input variables, it will inevitably encounter the problem of rule explosion. Different from the fuzzy inference method of single input rule module connection in the literature [58] to avoid the problem of rule explosion, we use information fusion to avoid this problem.

The four internal variables of the system discussed in this paper exhibit strong coupling and internal correlation, and the output information of the system has direct coupling, so the linear fusion function can be constructed to achieve dimensional reduction and simplify the fuzzy controller design. The information fusion technology in [59] is extended to the design of the GT2FGS-PID controller to prevent the problem of rule explosion. The specific process is as follows [59]:

1. *Construct the state feedback gain matrix* The quadratic optimal control theory is used to minimize the quadratic performance index J of the model by selecting the appropriate weighted matrices Q and R. The quadratic performance index J and state feedback gain matrix K_1 are as follows:

$$
J = \int_0^\infty [x^{\mathrm{T}}(t)Qx(t) + u_2^{\mathrm{T}}(t)Ru_2(t)]\mathrm{d}t \tag{34}
$$

$$
K_1 = [K_{x_1}\ K_{x_3}\ K_{x_2}\ K_{x_4}], \tag{35}
$$

where K_{x_1}, K_{x_2}, K_{x_3}, and K_{x_4} are the feedback coefficients of x_1, x_2, x_3, and x_4, respectively, while T represents the matrix transposition. The selection of matrices Q and R is based on the principle of improving the control performance and reducing the control energy. A higher value of the non-zero element

in the Q matrix results in a greater influence of its corresponding state variables on the system.

2. *Construct fusion functions* To reduce the input dimension, x_1 and x_2 are selected as control principal terms, so

$$\begin{aligned} u_2 &= K_1 \cdot x \\ &= K_{x_1} \cdot x_1 + K_{x_2} \cdot x_2 + K_{x_3} \cdot x_3 + K_{x_4} \cdot x_4 \\ &= K_{x_1}[x_1 + \frac{K_{x_3}}{K_{x_1}} \cdot x_3] + K_{x_2}[x_2 + \frac{K_{x_4}}{K_{x_2}} \cdot x_4] \\ &= K_{x_1} \cdot \tilde{x_1} + K_{x_2} \cdot \tilde{x_2}. \end{aligned} \tag{36}$$

The input and output equations of the fusion function are:

$$\begin{bmatrix} \tilde{x_1} \\ \tilde{x_2} \end{bmatrix} = \begin{bmatrix} 1 & 0 & \frac{K_{x_3}}{Kx_1} & 0 \\ 0 & 1 & 0 & \frac{Kx_4}{Kx_2} \end{bmatrix} \times \begin{bmatrix} x_1 \\ x_2 \\ x_3 \\ x_4 \end{bmatrix}. \tag{37}$$

Secondly, $\tilde{x_1}$ (denoted by e in Fig. 1) and $\tilde{x_2}$ (denoted by ec in Fig. 1) are selected for the input variables of the proposed GT2FGS-PID controller, and the PID parameters (K_p, K_i, and K_d) are selected as the output variables of the GT2FGS-PID controller.

Third, once the input and output variables have been determined, we empirically determine their domain, shape, and the number of membership functions. Each input and output is divided into three groups of linguistic variables, namely small (S), middle (M), and big (B). To achieve improved control performance and make the proposed controller achievable, the PSO algorithm is used to optimize the antecedents of the type-1 fuzzy gain scheduling PID (T1FGS-PID), interval type-2 fuzzy gain scheduling PID (IT2FGS-PID), and GT2FGS-PID controllers.

The FOU($\tilde{\tilde{A}}$) of $\tilde{x}_1$ and $\tilde{x}_2$ can be denoted by Eqs. (38) and (39) and Eqs. (40) and (41), respectively.

$$\text{LMF} = \begin{cases} \underline{\mu}_{\tilde{S}}(\tilde{x_1}') = \frac{1}{3}\tilde{x_1}' + \frac{5}{3},\ \tilde{x_1}' \in [-5,-2] \\ \underline{\mu}_{\tilde{S}}(\tilde{x_1}') = -\tilde{x_1}' - 1,\ \tilde{x_1}' \in (-2,-1] \\ \underline{\mu}_{\tilde{M}}(\tilde{x_1}') = \frac{2}{3}\tilde{x_1}' + 1,\ \tilde{x_1}' \in [-1.5,0] \\ \underline{\mu}_{\tilde{M}}(\tilde{x_1}') = -\frac{2}{3}\tilde{x_1}' + 1,\ \tilde{x_1}' \in [0,1.5] \\ \underline{\mu}_{\tilde{B}}(\tilde{x_1}') = \tilde{x_1}' - 2,\ \tilde{x_1}' \in [2,3] \\ \underline{\mu}_{\tilde{B}}(\tilde{x_1}') = \tilde{x_1}' + 4,\ \tilde{x_1}' \in [3,4] \\ = 0,\ \tilde{x_1}' \in (-\infty,-4) \cup \tilde{x_1}' \in (4,+\infty) \end{cases} \tag{38}$$

$$\text{UMF} = \begin{cases} \overline{\mu}_{\tilde{S}}(\tilde{x_1}') = \frac{1}{3}\tilde{x_1}' + 2,\ \tilde{x_1}' \in [-6,-3] \\ \overline{\mu}_{\tilde{S}}(\tilde{x_1}') = -\frac{1}{2}\tilde{x_1}' - \frac{1}{2},\ \tilde{x_1}' \in (-3,-1] \\ \overline{\mu}_{\tilde{M}}(\tilde{x_1}') = \frac{1}{3}\tilde{x_1}' + 1,\ \tilde{x_1}' \in [-3,0] \\ \overline{\mu}_{\tilde{M}}(\tilde{x_1}') = -\frac{1}{3}\tilde{x_1}' + 1,\ \tilde{x_1}' \in [0,3] \\ \overline{\mu}_{\tilde{B}}(\tilde{x_1}') = \frac{1}{2}\tilde{x_1}' - 2,\ \tilde{x_1}' \in [1,3] \\ \overline{\mu}_{\tilde{B}}(\tilde{x_1}') = -\frac{1}{3}\tilde{x_1}' + 2,\ \tilde{x_1}' \in [3,6] \\ = 0,\ \tilde{x_1}' \in (-\infty,-6) \cup \tilde{x_1}' \in (6,+\infty) \end{cases} \tag{39}$$

$$\text{LMF} = \begin{cases} \underline{\mu}_{\tilde{S}}(\tilde{x_2}') = \tilde{x_2}' + 3,\ \tilde{x_2}' \in [-3,-2] \\ \underline{\mu}_{\tilde{S}}(\tilde{x_2}') = -\tilde{x_2}' - 1,\ \tilde{x_2}' \in (-2,-1] \\ \underline{\mu}_{\tilde{M}}(\tilde{x_2}') = \tilde{x_2}' + 1,\ \tilde{x_2}' \in [-1,0] \\ \underline{\mu}_{\tilde{M}}(\tilde{x_2}') = -\tilde{x_2}' + 1,\ \tilde{x_2}' \in [0,1] \\ \underline{\mu}_{\tilde{B}}(\tilde{x_2}') = \tilde{x_2}' - 1,\ \tilde{x_2}' \in [1,2] \\ \underline{\mu}_{\tilde{B}}(\tilde{x_2}') = \tilde{x_2}' + 3,\ \tilde{x_2}' \in [2,3] \\ = 0,\ \tilde{x_2}' \in (-\infty,-3) \cup \tilde{x_2}' \in (3,+\infty) \end{cases} \tag{40}$$

$$\text{UMF} = \begin{cases} \overline{\mu}_{\tilde{S}}(\tilde{x_2}') = \frac{1}{3}\tilde{x_2}' + \frac{5}{3},\ \tilde{x_2}' \in [-6,-3] \\ \overline{\mu}_{\tilde{S}}(\tilde{x_2}') = -\frac{1}{2}\tilde{x_2}',\ \tilde{x_2}' \in (-2,0] \\ \overline{\mu}_{\tilde{M}}(\tilde{x_2}') = \frac{1}{2}\tilde{x_2}' + 1,\ \tilde{x_2}' \in [-2,0] \\ \overline{\mu}_{\tilde{M}}(\tilde{x_2}') = -\frac{1}{2}\tilde{x_2}' + 1,\ \tilde{x_2}' \in [0,2] \\ \overline{\mu}_{\tilde{B}}(\tilde{x_2}') = \frac{1}{2}\tilde{x_2}',\ \tilde{x_2}' \in [0,2] \\ \overline{\mu}_{\tilde{B}}(\tilde{x_2}') = -\frac{1}{3}\tilde{x_2}' + \frac{5}{3},\ \tilde{x_2}' \in [2,5] \\ = 0,\ \tilde{x_2}' \in (-\infty,-5) \cup \tilde{x_2}' \in (5,+\infty). \end{cases} \tag{41}$$

To make the GT2FGS-PID controller computation easier, five α planes are selected to represent the GT2-FS, where $\alpha_k = 0, 0.25, 0.5, 0.75, 1$. The membership functions used in the inputs are illustrated in Figs. 9 and 10. The upper and lower membership functions of the outputs are illustrated in Figs. 11, 12, and 13. Because the PID control theory is mature, we can design its rule directly according to the parameter regulation law of the PID control theory. For example, at the beginning of the control, a large control signal is needed to start the time rapidly. To generate a large control signal, a large proportional gain K_p, large integral gain K_i, and small differential gain K_d are required. Thus, the fuzzy rule is as follows:

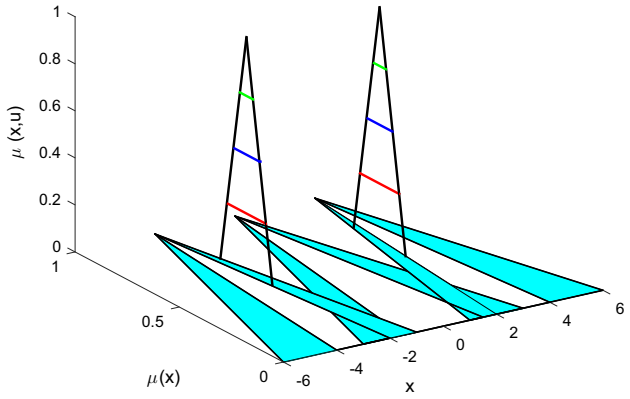

Fig. 9 Membership functions for $\tilde{x}_1$ with GT2-FS

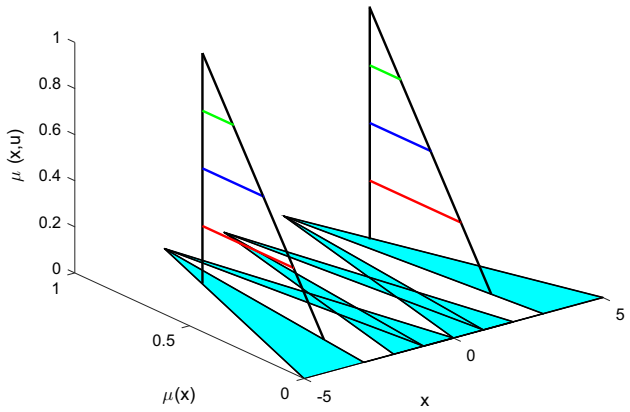

Fig. 10 Membership functions for $\tilde{x}_2$ with GT2-FS

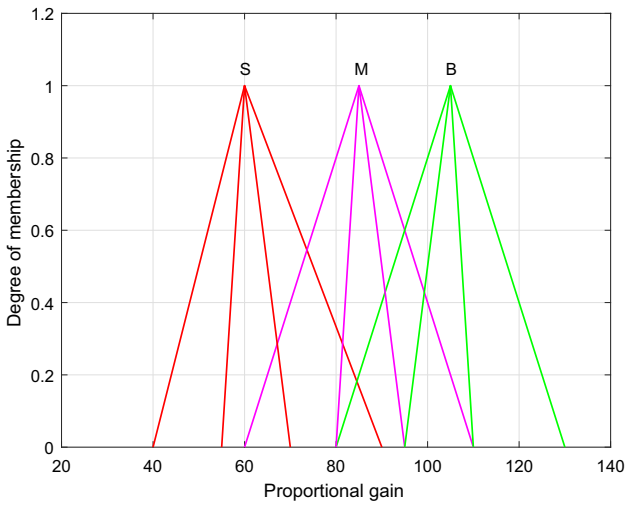

Fig. 11 Upper and lower membership functions for K_p

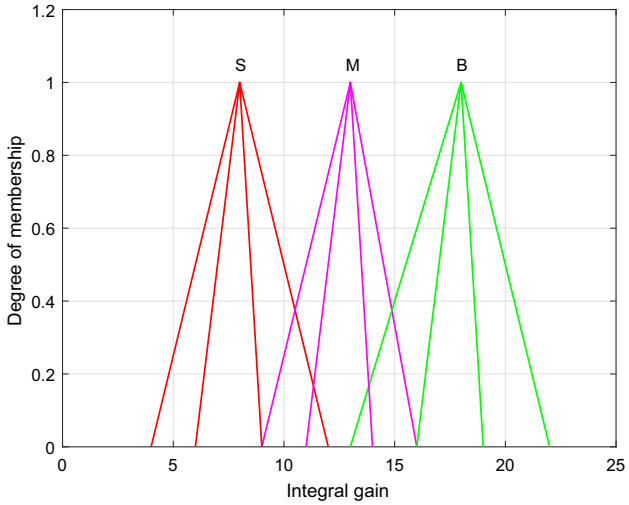

Fig. 12 Upper and lower membership functions for K_i

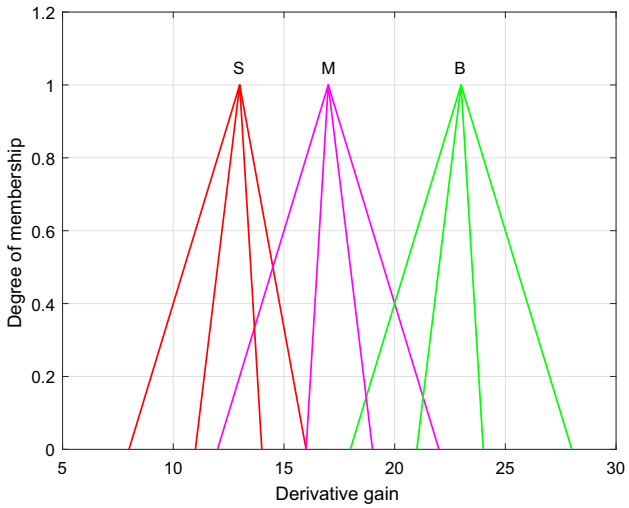

Fig. 13 Upper and lower membership functions for K_d

$$\begin{aligned} &\text{IF } \tilde{x_1} \text{ is } B \text{ and } \tilde{x_2} \text{ is } M, \text{THEN} \\ &\quad K_p \text{ is } B,\ K_i \text{ is } B,\ K_d \text{ is } S. \end{aligned} \tag{42}$$

When it is near the equilibrium point, to avoid deviation from the equilibrium state, a small proportional gain K_p, small integral gain K_i, and large differential gain K_d are required to construct a small control signal. Therefore, the fuzzy rule is as follows:

$$\begin{aligned} &\text{IF } \tilde{x_1} \text{ is } M \text{ and } \tilde{x_2} \text{ is } B, \text{THEN} \\ &\quad K_p \text{ is } S,\ K_i \text{ is } S,\ K_d \text{ is } B. \end{aligned} \tag{43}$$

Therefore, the specific rule base for K_p, K_i, and K_d of the PLI robot system is presented in Table 2.

Table 2 Rule base

$\tilde{x}_2$	$\tilde{x}_1$								
	K_p			K_i			K_d		
	S	M	B	S	M	B	S	M	B
S	M	S	M	B	S	B	M	B	M
M	B	M	B	B	M	B	S	B	S
B	M	S	M	M	S	M	M	B	M

Finally, the designed controller is applied to the PLI robot system. The corresponding simulation results will be presented in the following section.

4.3 Analysis of the GT2FGS-PID Controller

The controller proposed in this paper uses COS type-reduction as well as the average of end-points defuzzification. The rule base is as indicated as Table 2. Because the input primary and secondary membership functions are all triangles, the membership degree of the inputs share the structural pattern as illustrated in Fig. 14.

$$\begin{aligned}\underline{\mu}(x'_j) &= \frac{(x'_j + P_L^l - L_L^l)}{P_L^l} \\ \overline{\mu}(x'_j) &= \frac{(x'_j + P_U^l - L_U^l)}{P_U^l}\end{aligned} \tag{44}$$

Moreover, the firing interval can be expressed as follows:

$$\underline{f}_{\alpha_k}^l(x') = \prod_{j=1}^{p} a_{j,\alpha_k}^l(x'_j) \tag{45}$$

$$\overline{f}_{\alpha_k}^l(x') = \prod_{j=1}^{p} b_{j,\alpha_k}^l(x'_j), \tag{46}$$

where $\prod$ represents the continuous multiplication, and $a_{i,\alpha_k}^l(x'_i)$ and $b_{i,\alpha_k}^l(x'_i)$ can be computed by Eq. (24). The $c_l(\tilde{G}_{\alpha_k}^l)$ and $c_r(\tilde{G}_{\alpha_k}^l)$ are the centroids of consequents for level-α, and can be computed by Eqs. (47) and (48). Select m^l arbitrarily for each of the consequent GT2-FSs, and fix m_1^l and m_2^l at their $\alpha_k = 0$ values.

$$c_l(\tilde{G}_{\alpha_k}^l) = m_1^l + (m^l - m_1^l)\alpha_k \tag{47}$$

$$c_r(\tilde{G}_{\alpha_k}^l) = m_2^l - (m_2^l - m^l)\alpha_k \tag{48}$$

Thus, the outputs of the GT2-FLC, k_p, k_i, and k_d share the same structural pattern:

$$Y^{\cos}(x') = \frac{\sum_{k=1}^{k_{\max}} \alpha_k[(y_{l,\alpha_k}^{\cos}(x') + y_{r,\alpha_k}^{\cos}(x'))/2]}{\sum_{k=1}^{k_{\max}} \alpha_k}, \tag{49}$$

where

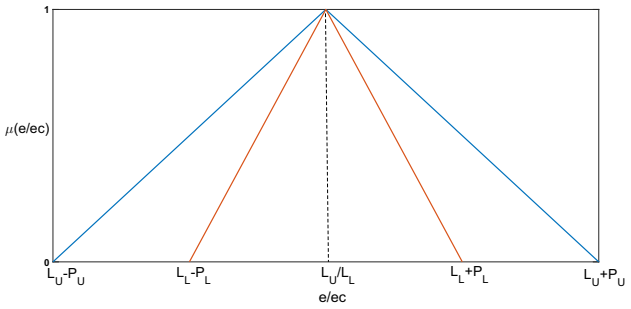

Fig. 14 Triangular membership function for inputs

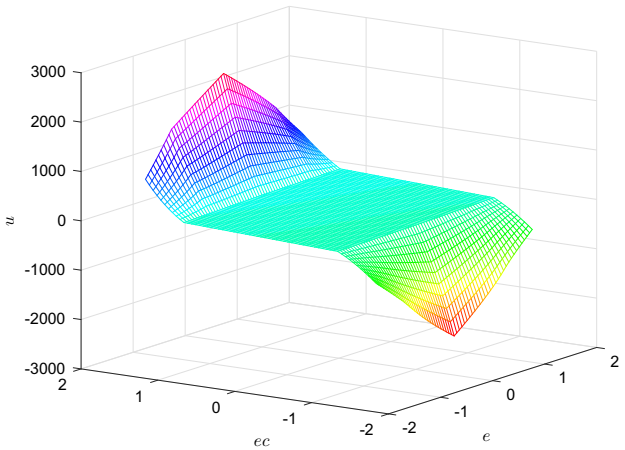

Fig. 15 Control surface of GT2FGS-PID controller

$$\begin{aligned}y_{l,\alpha_k}^{\cos}(x') &= \frac{\sum_{i=1}^{L} c_l(\tilde{G}_{\alpha_k}^l)\overline{f}_{\alpha_k}^i(x') + \sum_{i=L+1}^{M} c_l(\tilde{G}_{\alpha_k}^l)\underline{f}_{\alpha_k}^i(x')}{\sum_{i=1}^{L} \overline{f}_{\alpha_k}^i(x') + \sum_{i=L+1}^{M} \underline{f}_{\alpha_k}^i(x')} \\ y_{r,\alpha_k}^{\cos}(x') &= \frac{\sum_{i=1}^{R} c_r(\tilde{G}_{\alpha_k}^l)\underline{f}_{\alpha_k}^i(x') + \sum_{i=R+1}^{M} c_r(\tilde{G}_{\alpha_k}^l)\overline{f}_{\alpha_k}^i(x')}{\sum_{i=1}^{R} \underline{f}_{\alpha_k}^i(x') + \sum_{i=R+1}^{M} \overline{f}_{\alpha_k}^i(x')}.\end{aligned} \tag{50}$$

In summary, the output of the GT2FGS-PID controller is

$$u(t) = k_p(e, ec)e(t) + k_i(e, ec)\int_0^t e(t')\mathrm{d}t' + k_d(e, ec)ec(t). \tag{51}$$

Therefore, the control surface of the proposed controller can be illustrated by Figs. 15 and 16. From the control surface, it can be observed that the proposed GT2FGS-PID is very smooth near the equilibrium point, which indicates that the proposed controller has the potential to obtain superior control performance.

Remark 2 The outputs of the GT2-FLC (K_p, K_i, and K_d) are nonlinear functions with respect to the inputs. That is, the GT2FGS-PID controller is equivalent to a nonlinear PID controller with variable gains.

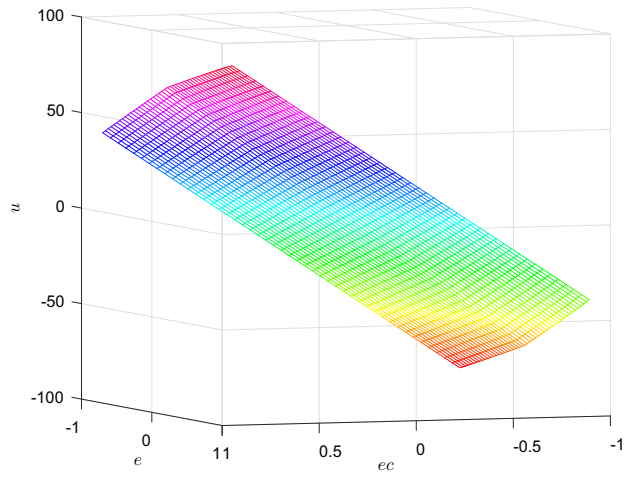

Fig. 16 Partial view of control surface of GT2FGS-PID controller

5 Simulation

In this section, the PLI robot system is simulated based on MATLAB by four controllers: the conventional PID, T1FGS-PID controller, IT2FGS-PID controller, and GT2FGS-PID controller. The original position is $x = [0.3\ 0\ -0.3145\ 0]^{\mathrm{T}}$ and the control task involves returning the PIL robot to its balance position $x = [0\ 0\ 0\ 0]^{\mathrm{T}}$ through the self-balancing mechanism. For a more comprehensive understanding of the proposed GT2FGS-PID controller performance and robustness, four simulation tasks are performed by the PLI robot system. Consider the matrices Q, R, and K_1, as follows:

$$Q = \mathrm{diag}[250, 150, 150, 50], R = 10 \tag{52}$$

$$K_1 = [-9.4663\ \ -6.773928\ 28.2025\ 7.8361]. \tag{53}$$

Moreover, three types of evaluation functions (ISE, IAE, and ITAE) are used to evaluate the control performance of the three control methods quantitatively, and these are defined by Eqs. (54) to (56).

$$\mathrm{ISE} = \sum_{n=1}^{k} e(nT)^2 T \tag{54}$$

$$\mathrm{IAE} = \sum_{n=1}^{k} |e(nT)| T \tag{55}$$

$$\mathrm{ITAE} = \sum_{n=1}^{k} |e(nT)| nT^2, \tag{56}$$

where T is the sampling time.

Furthermore, the PSO algorithm is considered to optimize the antecedents of the T1FGS-PID, IT2FGS-PID, and GT2FGS-PID controllers, and it should be noted that the shape of the secondary function of the GT2-FS is also optimized. The selection of the objective function is

$$\mathrm{Obj\_}f = \omega_1 \sum_{n=1}^{k} |e(nT)| T + \omega_2 \sum_{n=1}^{k} |e(nT)| nT^2, \tag{57}$$

where both w_1 and w_2 are equal to 0.5 in this study.

Remark 3 It should be noted that the optimal parameters are obtained by offline optimization of PSO algorithm. To better apply it to the real system, we refer to references [60–62]. In the future research, we will use self-organizing fuzzy controller to improve the online application ability of the controller.

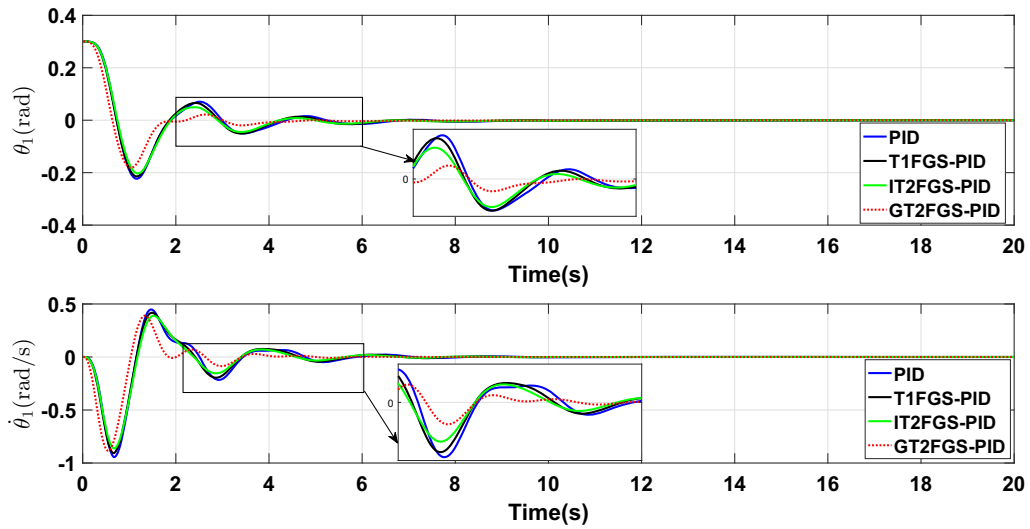

Fig. 17 Response of PLI robot for normal case

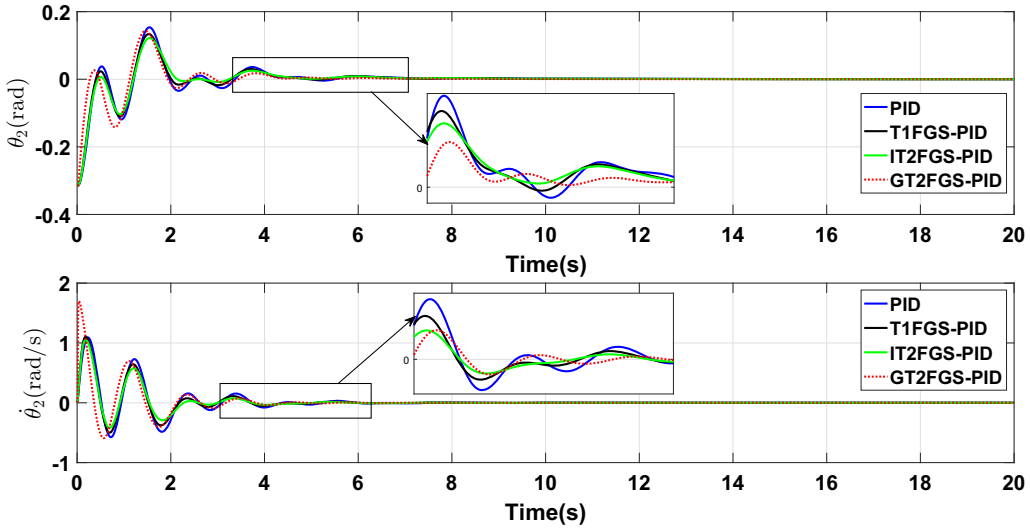

Fig. 18 Response of PLI robot for normal case

Table 3 Performance index results for normal case

Performance index	x_1				x_3			
	PID	T1FGS-PID	IT2FGS-PID	GT2FGS-PID	PID	T1FGS-PID	IT2FGS-PID	GT2FGS-PID
ISE	0.070	0.067	0.064	0.048	0.029	0.025	0.024	0.021
IAE	0.433	0.418	0.395	0.282	0.025	0.228	0.220	0.205
ITAE	0.791	0.728	0.65	0.329	0.552	0.467	0.440	0.330

5.1 Normal Case

Figures 17 and 18 illustrate the responses of the PLI robot for the normal case. The original position is $x = [0.3\ 0\ -0.3145\ 0]^{\mathrm{T}}$ and the desired balance position is $x = [0\ 0\ 0\ 0]^{\mathrm{T}}$. In this case, we assume that the external interference is equal to 0 ($\tau_1 = 0$ N). It can be observed that the GT2FGS-PID controller has a smaller overshoot and superior performance compared to other controllers from Figs. 17 and 18 as well as Table 3.

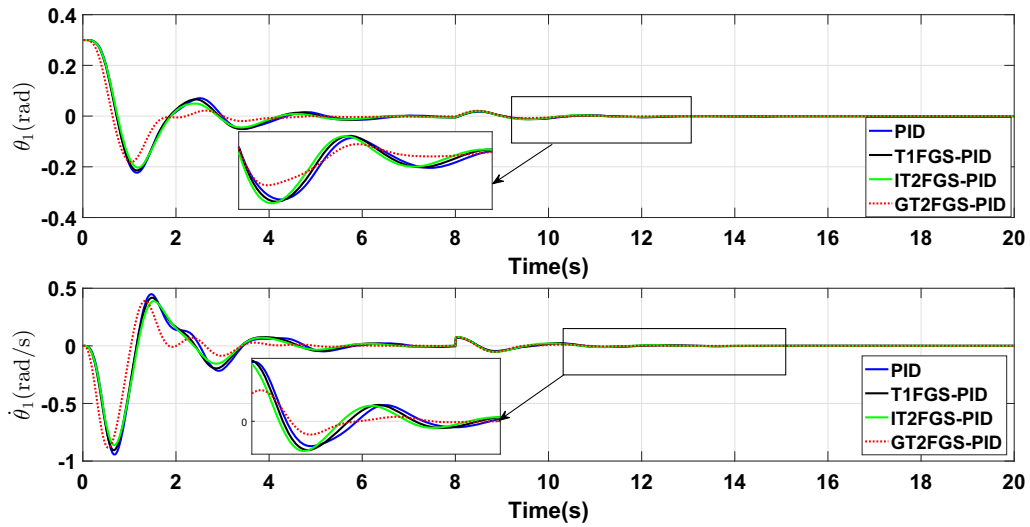

Fig. 19 Response of PLI robot when disturbance value is $\tau_1 = 100$ N

5.2 External Disturbance

Figures 19 and 20 illustrate the responses of the PLI robot system for the external disturbance $\tau_1 = 100$ N. It can be observed that, although the external interference is sufficiently large, the system can remain stable quickly, and exhibits strong robustness. In particular, according to Table 4, the GT2FGS-PID controller obtains the best results. Moreover, when the external disturbance τ_1 is increased to 500 N, it can be observed from Figs. 21 and 22 as well as Table 5 that the GT2FGS-PID controller can still exhibit the best control performance.

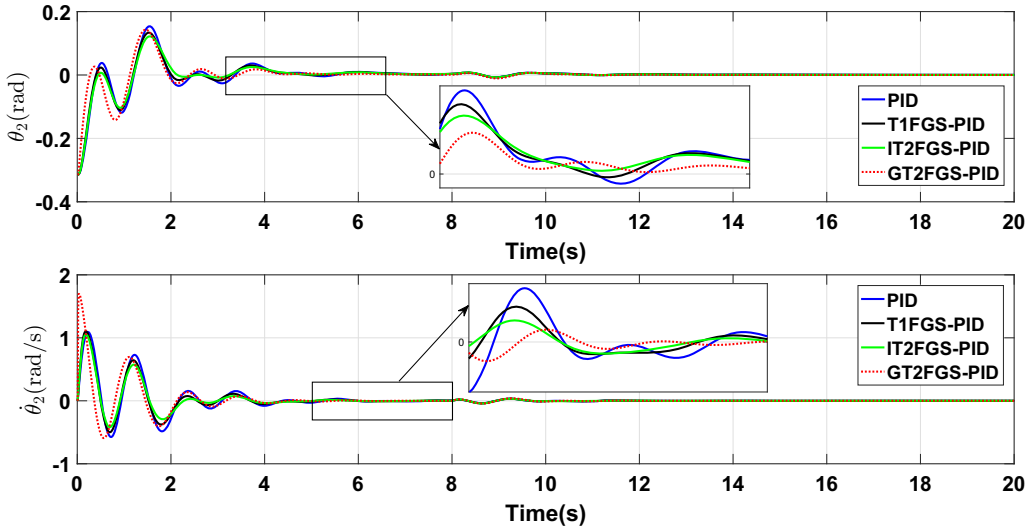

Fig. 20 Response of PLI robot when disturbance value is $\tau_1 = 100$ N

Table 4 Performance index results with external disturbance ($\tau_1 = 100$ N)

Performance index	x_1				x_3			
	PID	T1FGS-PID	IT2FGS-PID	GT2FGS-PID	PID	T1FGS-PID	IT2FGS-PID	GT2FGS-PID
ISE	0.070	0.067	0.065	0.048	0.029	0.025	0.024	0.021
IAE	0.450	0.438	0.415	0.302	0.267	0.236	0.228	0.218
ITAE	0.964	0.921	0.844	0.526	0.633	0.550	0.521	0.450

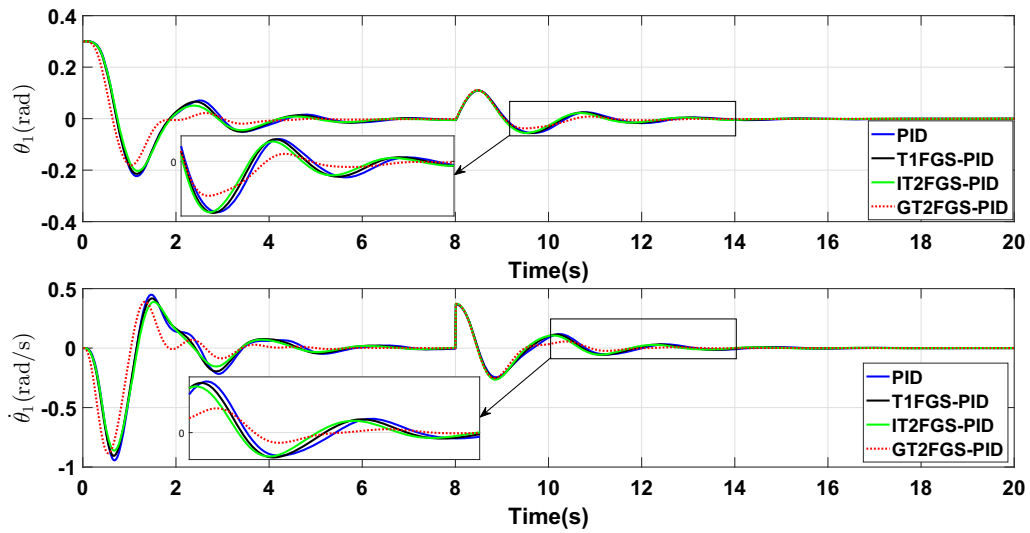

Fig. 21 Response of PLI robot when disturbance value is $\tau_1 = 500$ N

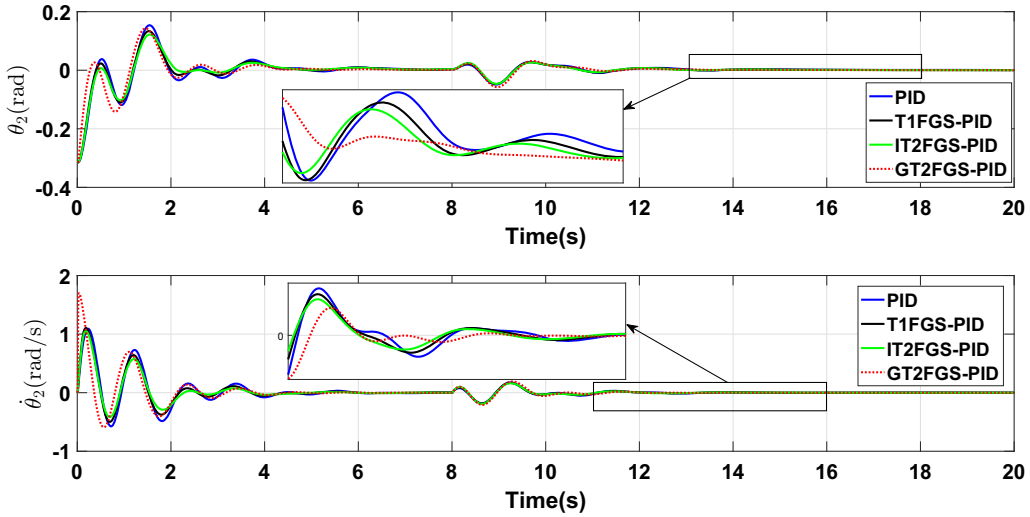

Fig. 22 Response of PLI robot when disturbance value is $\tau_1 = 500$ N

Table 5 Performance index results with external disturbance ($\tau_1 = 500$ N)

Performance index	x_1				x_3			
	PID	T1FGS-PID	IT2FGS-PID	GT2FGS-PID	PID	T1FGS-PID	IT2FGS-PID	GT2FGS-PID
ISE	0.079	0.076	0.073	0.055	0.031	0.026	0.026	0.023
IAE	0.579	0.562	0.531	0.401	0.323	0.289	0.278	0.275
ITAE	2.228	2.124	1.961	1.449	1.208	1.083	1.027	1.022

5.3 Uncertainty in Mass

For a more comprehensive understanding of the robust performance of the GT2FGS-PID controller, we change the quality within a certain range ($\Delta m_1 = 20$ kg, $\Delta m_2 = 10$ kg). Figures 23 and 24 as well as Table 6 demonstrate that the proposed controller can completely overcome the change in parameters in the system.

5.4 With White Noise

Figure 25 illustrates the white noise added to the input $\tilde{x_1}$. Figures 26, 27 and Table 7 illustrate the responses of the

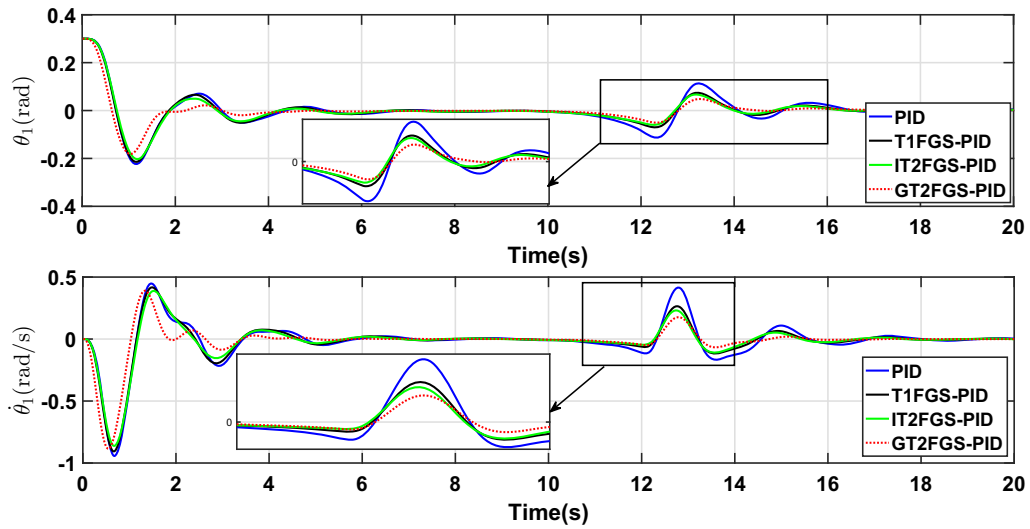

Fig. 23 Response of PLI robot with uncertainty in mass

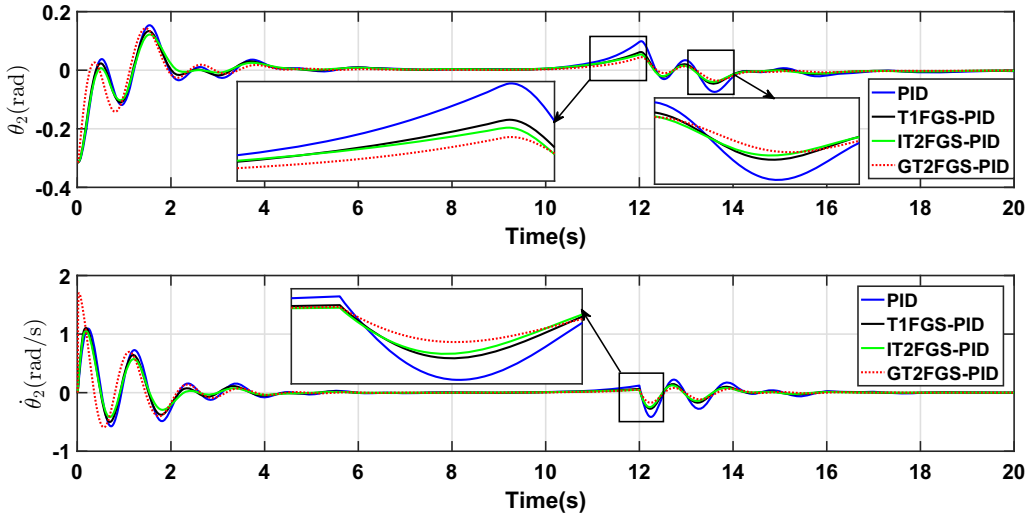

Fig. 24 Response of PLI robot with uncertainty in mass

Table 6 Performance Index results with uncertainty in mass

Performance index	x_1				x_3			
	PID	T1FGS-PID	IT2FGS-PID	GT2FGS-PID	PID	T1FGS-PID	IT2FGS-PID	GT2FGS-PID
ISE	0.088	0.074	0.708	0.051	0.038	0.029	0.027	0.021
IAE	0.705	0.591	0.550	0.397	0.441	0.347	0.331	0.296
ITAE	4.409	3.012	2.691	1.843	2.939	2.019	1.897	1.527

robot with white noise. It can be observed that the advantages of the GT2FGS-PID controller are reflected in the face of noise, small amplitude, and short stabilization time, among others.

Remark 4 In each simulation diagram, it can be observed that the control trends of the four controllers are consistent. This is because the fuzzy controller is responsible for online adjustment of the three parameters K_p, K_i, and K_d, following which the PID controller performs parameter integration and produces the control output. The significance of using FLC controllers lies in two points. First, based on this uncertain and inaccurate nonlinear model, the fuzzy controller can use human experience to set and adjust the parameters of the PID controller online for improved control. Second, in the face of high uncertainty, the FLC controller can exploit its own advantages and reduce the impact of disturbance.

Remark 5 The GT2-FLC is superior to the IT2-FLC and T1-FLC in terms of two aspects. First, the GT2-FLC itself has greater degrees of freedom, which makes it possible to improve the control performance. Second, as an extension of the IT2-FLC, the GT2-FLC control performance is no worse than that of the IT2-FLC, even if no improved parameters are determined to distinguish the difference between the two FLCs.

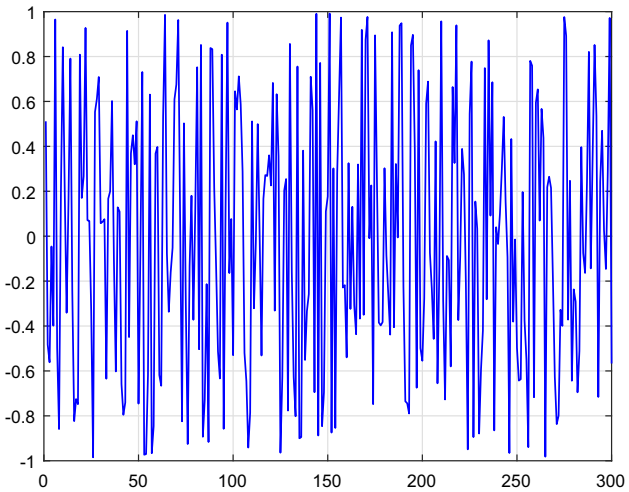

Fig. 25 White noise added to input $\tilde{x_1}$

Remark 6 Since the controlled object of this paper is the same as the literature [8], we compare the results in this paper with that in the literature [8]. Compared with the literature [8], there are two main differences: (1) [8] uses a

linear mathematical model, and this paper uses a nonlinear mathematical model in simulation. In fact, the control method based on linear model can hardly be used in PLI robot system; (2) Literature [8] uses adaptive gain-scheduled backstepping control method to PLI robot system. However, the premise of the effectiveness of the adaptive gain-scheduled backstepping control method is that the mathematical model of the PLI robot system with linear form is accurate. However, the mathematical model of PLI robot system with linear form ignores many factors, so it is difficult to apply to practical system. The control method in this paper does not depend entirely on the precise mathematical model, and to improve the realizability of the controller, the PSO algorithm is used to solve the optimal parameters. Therefore, the proposed method has the potential to be applied to practical systems.

6 Conclusions and Future Work

6.1 Conclusions

In this paper, a GT2FGS-PID controller that does not depend entirely on a mathematical model has been proposed to adjust the PLI robot system, because it is difficult to construct a precise mathematical model of the PLI robot system in actual situations. Using information fusion technology, the four-state variables are converted into error

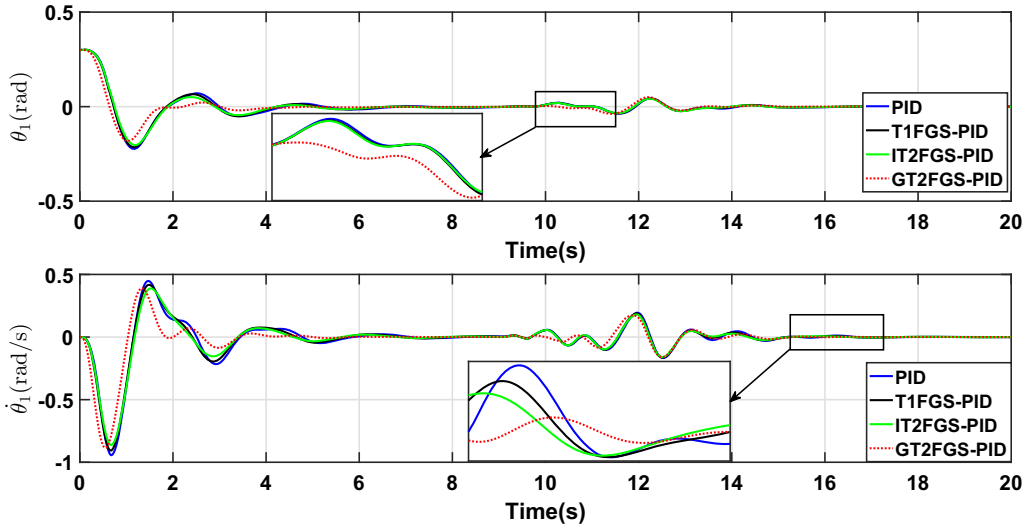

Fig. 26 Response of PLI robot with white noise

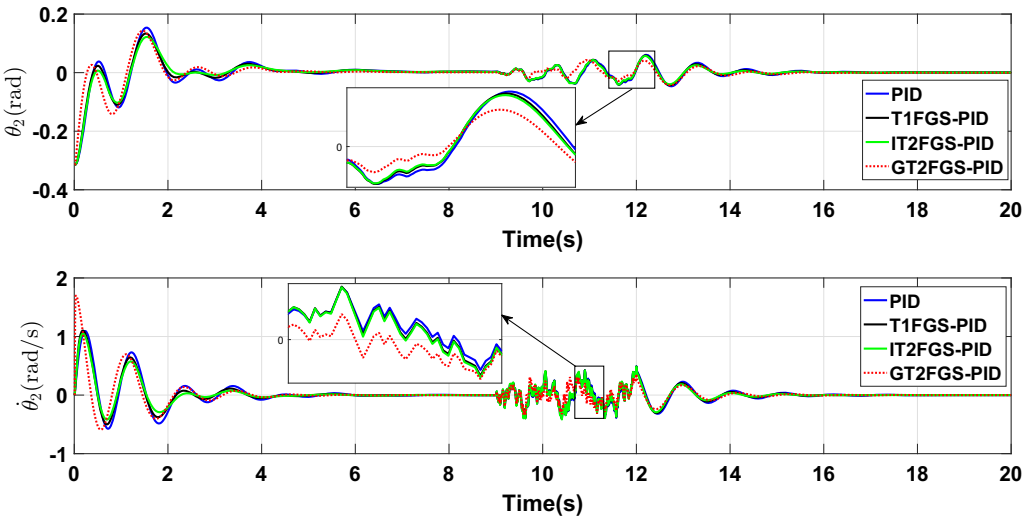

Fig. 27 Response of PLI robot with white noise

Table 7 Performance index results with white noise

Performance index	x_1				x_3			
	PID	T1FGS-PID	IT2FGS-PID	GT2FGS-PID	PID	T1FGS-PID	IT2FGS-PID	GT2FGS-PID
ISE	0.072	0.069	0.066	0.050	0.033	0.028	0.027	0.023
IAE	0.501	0.485	0.459	0.347	0.370	0.332	0.317	0.289
ITAE	1.639	1.564	1.446	1.131	1.904	1.710	1.597	1.341

and error change rate, so that the controller can be designed conveniently and the rule explosion problem can be avoided. The PSO algorithm is used to solve the problem where by the GT2-FLS parameters are difficult to adjust effectively. The GT2FGS-PID controller is compared to the PID, T1FGS-PID and IT2FGS-PID controllers in the absence of disturbance and various disturbances. The comparison results demonstrate that the proposed GT2FGS-PID provides the best control effect and a strong anti-interference ability.

6.2 Future Work

With the completion of this work, we have several ideas for future work:

1. Constant exploration of the stability conditions of the GT2FGS-PID controller will be undertaken to make the theory more complete.
2. Combining a GT2-FLC with a fractional PID could be an effective concept. The fractional-order PID is a generalization of the integer-order PID, and the fractional-order PID has two more degrees of freedom than the integer-order PID, so its flexibility is superior. This also means that it can be combined with the GT2-FLC and applied to the robot for improved control performance.
3. To reduce the computational complexity of the GT2-FLS, the α-plane method is used in this study. A higher number of α-planes selected will yield more accurate results. However, as the number of α-planes increases, the computational complexity increases significantly, so determining a balance between the two is also a challenging task.

Funding This work is supported by the National Key R&D Program of China (2018YFB1307401) and the National Natural Science Foundation of China (61703291).

References

1. Jin, L., Li, S., Luo, X., et al.: Neural dynamics for cooperative control of redundant robot manipulators. IEEE Trans. Ind. Inform. **14**(9), 3812–3821 (2018)
2. Yang, C., Wu, H., Li, Z., et al.: Mind control of a robotic arm with visual fusion technology. IEEE Trans. Ind. Inform. **14**(9), 3822–3830 (2018)
3. Li, J., Zhang, Y., Li, S., et al.: New discretization-formula-based zeroing dynamics for real-time tracking control of serial and parallel manipulators. IEEE Trans. Ind. Inform. **14**(8), 3416–3425 (2018)
4. Shin, S.Y., Lee, J.J.: Fuzzy sliding mode control for an underactuated system with mismatched uncertainties. Artif. Life Robot. **15**(3), 355–358 (2010)
5. Li, H., Savkin, A.V.: Wireless sensor network based navigation of micro flying robots in the industrial internet of things. IEEE Trans. Ind. Inform. **14**(8), 3524–3533 (2018)
6. Choukchou-Braham, A., Cherki, B., Djemai, M., et al.: Analysis and control of underactuated mechanical systems. Springer, Berlin (2013)
7. Dian, S., Hoang, S., Pu, M., et al.: Gain scheduling based backstepping control for motion balance adjusting of a power-line inspection robot[C]. In: Control Conference IEEE, pp. 441–446 (2016)
8. Dian, S., Chen, L., Hoang, S., et al.: Dynamic balance control based on an adaptive gain-scheduled backstepping scheme for power-line inspection robots. IEEE/CAA J. Automat. Sinica **6**(1), 198–208 (2019)
9. Huang, J., Ding, F., Wang, Y.: Sliding mode control with nonlinear disturbance observer for a class of underactuated system. In: Control Conference IEEE, pp. 541–546 (2013)
10. Xin, X., Liu, Y.: Trajectory tracking control of variable length pendulum by partial energy shaping. Commun. Nonlinear Sci. Numer. Simul. **19**(5), 1544–1556 (2014)
11. Fang, Y., Ma, B., Wang, P., et al.: A motion planning-based adaptive control method for an underactuated crane system. IEEE Trans. Control Syst. Technol. **20**(1), 241–248 (2011)
12. Huang, M., Xian, B., Diao, C., et al.: Adaptive tracking control of underactuated quadrotor unmanned aerial vehicles via backstepping. In: American Control Conference IEEE, pp. 2076–2081 (2010)
13. Cherrat, N., Boubertakh, H., Arioui, H.: An adaptive fuzzy PID control for a class of uncertain nonlinear underactuated systems. In: International Conference on Modelling, Identification and Control. IEEE, pp. 677-682 (2017)
14. Li, Y., Liu, L., Feng, G.: Robust adaptive output feedback control to a class of non-triangular stochastic nonlinear systems. Automatica **89**, 325–332 (2018)

15. Tran, H.D., Guan, Z.H., Dang, X.K., et al.: A normalized PID controller in networked control systems with varying time delays. ISA Trans. **52**(5), 592–599 (2013)
16. Kim, J.H., Oh, S.J.: A fuzzy PID controller for nonlinear and uncertain systems. Soft Comput. **4**(2), 123–129 (2000)
17. Qiao, W.Z., Mizumoto, M.: PID type fuzzy controller and parameters adaptive method. Fuzzy Sets Syst. **78**(1), 23–35 (1996)
18. Carvajal, J., Chen, G., Ogmen, H.: Fuzzy PID controller: design, performance evaluation, and stability analysis. Inform. Sci. **123**(3–4), 249–270 (2000)
19. Alavandar, S., Nigam, M.J.: Fuzzy PD+ I control of a six DOF robot manipulator. Ind. Robot **35**(2), 125–132 (2008)
20. Kumbasar, T., Hagras, H.: A self-tuning zSlices-based general type-2 fuzzy PI controller. IEEE Trans. Fuzzy Syst. **23**(4), 991–1013 (2015)
21. Mendel, J.M.: Type-2 fuzzy sets and systems: an overview. IEEE Comput. Intell. Mag. **2**(1), 20–29 (2007)
22. El-Bardini, M., El-Nagar, A.M.: Interval type-2 fuzzy PID controller for uncertain nonlinear inverted pendulum system. ISA Trans. **53**(3), 732–743 (2014)
23. Castillo, O., Melin, P.: Type-2 fuzzy logic: theory and applications. Springer, Berlin (2008)
24. Mendel, J.M., John, R.I., Liu, F.: Interval type-2 fuzzy logic systems made simple. IEEE Press, New York (2006)
25. Hagras, H.: Type-2 FLCs: a new generation of fuzzy controllers. Comput. Intell. Mag. IEEE **2**(1), 30–43 (2007)
26. Zhao, T., Dian, S.: State feedback control for interval type-2 fuzzy systems with time-varying delay and unreliable communication links. IEEE Trans. Fuzzy Syst. **26**(2), 951–966 (2018)
27. Zhao, T., Dian, S.: Delay-dependent stabilization of discrete-time interval type-2 T-S fuzzy systems with time-varying delay. J. Franklin Instit. **354**(3), 1542–1567 (2017)
28. Lam, H.K., Li, H., Deters, C., et al.: Control design for interval type-2 fuzzy systems under imperfect premise matching. IEEE Trans. Ind. Elect. **61**(2), 956–968 (2014)
29. Li, H., Yin, S., Pan, Y., et al.: Model reduction for interval type-2 Takagi–Sugeno fuzzy systems. Automatica **61**(11), 308–314 (2015)
30. Castillo, O., Melin, P.: Intelligent systems with interval type-2 fuzzy logic. Int. J. Innov. Comput. Inform. Control **4**(4), 771–783 (2008)
31. Jhang, J.Y., Lin, C.J., Lin, C.T., et al.: Navigation control of mobile robots using an interval type-2 fuzzy controller based on dynamic-group particle swarm optimization. Int. J. Control Automat. Syst. **16**(5), 2446–2457 (2018)
32. Huang, J., Ri, M.H., Wu, D., et al.: Interval type-2 fuzzy logic modeling and control of a mobile two-wheeled inverted pendulum. IEEE Trans. Fuzzy Syst. **26**(4), 2030–2038 (2018)
33. Eyoh, I., John, R., De Maere, G.: Interval type-2 A-intuitionistic fuzzy logic for regression problems. IEEE Trans. Fuzzy Syst. **26**(4), 2396–2408 (2018)
34. Eyoh, I., John, R., De Maere, G., et al.: Hybrid learning for interval type-2 intuitionistic fuzzy logic systems as applied to identification and prediction problems. IEEE Trans. Fuzzy Syst. **26**(5), 2672–2685 (2018)
35. Ontiveros-Robles, E., Melin, P., Castillo, O.: Comparative analysis of noise robustness of type 2 fuzzy logic controllers. Kybernetika **54**(1), 175–201 (2018)
36. Zhao, T., Liu, J., Dian, S.: Finite-time control for interval type-2 fuzzy time-delay systems with norm-bounded uncertainties and limited communication capacity. Inform. Sci. **483**, 153–173 (2019)
37. Li, C., Yi, J., Wang, H., et al.: Interval data driven construction of shadowed sets with application to linguistic word modelling. Inform. Sci. **507**, 503–521 (2020)
38. Sanchez, M.A., Castillo, O., Castro, J.R.: Generalized type-2 fuzzy systems for controlling a mobile robot and a performance comparison with interval type-2 and type-1 fuzzy systems. Pergamon Press, Inc, Oxford (2015)
39. Castillo, O., Amador-Angulo, L., Castro, J.R., et al.: A comparative study of type-1 fuzzy logic systems, interval type-2 fuzzy logic systems and generalized type-2 fuzzy logic systems in control problems. Inform. Sci. **354**, 257–274 (2016)
40. Tai, K., El-Sayed, A.R., Biglarbegian, M., et al.: Review of recent type-2 fuzzy controller applications. Algorithms **9**(2), 39 (2016)
41. Ontiveros, E., Melin, P., Castillo, O.: High order α-planes integration: a new approach to computational cost reduction of general type-2 fuzzy systems. Eng. Appl. Artif. Intell. **74**, 186–197 (2018)
42. Castillo, O., Amador-Angulo, L.: A generalized type-2 fuzzy logic approach for dynamic parameter adaptation in bee colony optimization applied to fuzzy controller design. Inform. Sci. **460–461**, 476–496 (2018)
43. Ghaemi, M., Hosseini-Sani, S.K., Khooban, M.H.: Direct adaptive general type-2 fuzzy control for a class of uncertain nonlinear systems. IET Sci. Meas. Technol. **8**(6), 518–527 (2014)
44. Castillo, O., Cervantes, L., Soria, J., et al.: A generalized type-2 fuzzy granular approach with applications to aerospace. Inform. Sci. **354**, 165–177 (2016)
45. Cervantes, L., Castillo, O.: Type-2 fuzzy logic aggregation of multiple fuzzy controllers for airplane flight control. Inform. Sci. **324**, 247–256 (2015)
46. Xie, X., Yue, D., Peng, C.: Multi-instant observer design of discrete-time fuzzy systems: a ranking-based switching approach. IEEE Trans. Fuzzy Syst. **25**(5), 1281–1292 (2017)
47. Chang, X.H.: Robust nonfragile H_∞ fuzzy systems with linear fractional parametric uncertainties. IEEE Trans. Fuzzy Syst. **20**(6), 1001–1011 (2012)
48. Mendel, J.M.: Uncertain rule-based fuzzy systems. Introduction and new directions, vol. 684. Springer, Berlin (2017)
49. Liang, Q., Mendel, J.M.: Interval type-2 fuzzy logic systems: theory and design[J]. IEEE Transactions on Fuzzy systems **8**(5), 535–550 (2000)
50. Aisbett, J., Rickard, J.T., Morgenthaler, D.G.: Type-2 fuzzy sets as functions on spaces. IEEE Trans. Fuzzy Syst. **18**(4), 841–844 (2010)
51. Mendel, J.M., Liu, F., Zhai, D.: α-Plane representation for type-2 fuzzy sets: theory and applications. IEEE Trans. Fuzzy Syst. **17**(5), 1189–1207 (2009)
52. Dubois, B.P.H.: Fuzzy sets and systems: theory and applications. Academic Press, New York (1980)
53. Mendel, J.M.: General type-2 fuzzy logic systems made simple: a tutorial. IEEE Trans. Fuzzy Syst. **22**(5), 1162–1182 (2014)
54. Karnik, N.N., Mendel, J.M.: Introduction to type-2 fuzzy logic systems. In: 1998 IEEE International Conference on Fuzzy Systems Proceedings IEEE World Congress on Computational Intelligence (Cat. No. 98CH36228). IEEE **2**, 915–920 (1998)
55. Wu, H., Mendel, J.M.: Uncertainty bounds and their use in the design of interval type-2 fuzzy logic systems. IEEE Trans. Fuzzy Syst. **10**(5), 622–639 (2002)
56. Craig, J.J.: Introduction to robotics: mechanics and control, 3/E. Pearson Education India, Oxford (2009)
57. Li, X.J., Yang, G.H.: Fault detection in finite frequency domain for Takagi–Sugeno fuzzy systems with sensor faults. IEEE Trans. Cybern. **44**(8), 1446–1458 (2013)
58. Li, C., Gao, J., Yi, J., et al.: Analysis and design of functionally weighted single-input-rule-modules connected fuzzy inference systems. IEEE Trans. Fuzzy Syst. **26**(1), 56–71 (2016)
59. Wang, L., Zheng, S., Wang, X., et al.: Fuzzy control of a double inverted pendulum based on information fusion. In: 2010

International Conference on Intelligent Control and Information Processing. IEEE, pp. 327–331 (2010)
60. Han, H.G., Liu, H.X., Liu, Z., et al.: Fault detection of sludge bulking using a self-organizing type-2 fuzzy-neural-network. Control Eng. Practice **90**, 27–37 (2019)
61. Han, H.G., Wu, X.L., Liu, Z., et al.: Design of self-organizing intelligent controller using fuzzy neural network. IEEE Trans. Fuzzy Syst. **26**(5), 3097–3111 (2017)
62. Han, H., Wu, X., Zhang, L., et al.: Self-organizing RBF neural network using an adaptive gradient multiobjective particle swarm optimization. IEEE Trans. Cybern. **49**(1), 69–82 (2017)

Tao Zhao received his B.S. degree in mathematics and applied mathematics and Ph.D. degree in systems engineering from Southwest Jiaotong University, Chengdu, China, in 2010 and 2015, respectively. He is currently an associate professor in the College of Electrical Engineering, Sichuan University. His current research interests include type-2 fuzzy set theory and system design, rough sets, and intelligent control.

Yao Chen received her B.S. degree from Chengdu University in 2017. Now she is pursuing the M.S. degree in control engineering from Sichuan University, China. Her research interests include fuzzy control, intelligent control and their applications.

Songyi Dian received his Bachelor and M.S. degrees of Control Engineering from Sichuan University, China in 1996 and 2002, respectively. He received his Ph.D degree in Nanomechanics Engineering from Tohoku University, Japan in 2009. He is currently a professor in the College of Electrical Engineering, Sichuan University. His current research interests include advanced control methods and intelligent signal processing, power-electronics system and its control, motion control and robotic control.

Rui Guo received his B.S., M.S. and Ph.D. degrees of Mechanical Engineering from Harbin Institute of Technology, China in 2001, 2003 and 2007, respectively. He is currently a professor of engineering in the State Grid Shandong Electric Power Company, China. His current research interests include advanced control methods and intelligent robot for power industry.

Shengchuan Li graduated from Harbin University of Technology in 1991. He is currently a professor of engineering in the Electric Power Research Institute of State Grid Liaoning Electric Power Co., Ltd., China. His research interests include operation and maintenance of substation equipment and application of artificial intelligence in power grid.